

# Transient hysteresis and inherent stochasticity in gene regulatory networks

M. Pájaro<sup>1\*</sup>, I. Otero-Muras<sup>1\*</sup>, C. Vázquez<sup>2</sup> & A. A. Alonso<sup>1</sup>

<sup>1</sup>*BioProcess Engineering Group, IIM-CSIC. Spanish National Research Council. Eduardo Cabello 6, 36208 Vigo, Spain*

<sup>2</sup>*Department of Mathematics, University of A Coruña. Campus Elviña s/n, 15071 A Coruña, Spain*

*\* These authors contributed equally to this work.*

Cell fate determination, the process through which cells commit to differentiated states is commonly mediated by gene regulatory motifs with mutually exclusive expression states. The classical deterministic picture for cell fate determination includes bistability and hysteresis, which enables the persistence of the acquired cellular state after withdrawal of the stimulus, ensuring a robust cellular response. However, the stochasticity inherent to gene expression dynamics is not compatible with hysteresis, since the stationary solution of the governing Chemical Master Equation does not depend on the initial conditions. In this work, we provide a quantitative description of a transient hysteresis phenomenon that reconciles experimental evidence of hysteretic behaviour in gene regulatory networks with their inherent stochasticity. Under sufficiently slow dynamics, the dependency of the non-stationary solutions on the initial state of the cells can lead to what we denote here as transient hysteresis. To quantify this phenomenon, we provide an estimate of the convergence rate to the equilibrium. We also introduce the equation of a natural landscape capturing the evolution

of the system that, unlike traditional cell fate potential landscapes, is compatible with the notion of coexistence at the microscopic level.

## 1 Introduction

In a deterministic description, binary decision making is attributed to the irreversible state transition between two mutually exclusive stable steady states in response to a signal. This state transition is usually governed by regulatory motifs with the capacity for bistability and hysteresis<sup>1</sup>, thus ensuring that the system does not switch back immediately when the signal is removed<sup>2</sup>.

The stochastic dynamic behaviour of a gene regulatory network is governed by a Chemical Master Equation (CME), which describes the time evolution of the probability distribution of the system state. The stationary solution of the CME is unique and independent on the initial state of the system<sup>3</sup> and therefore, incompatible with memory effects or hysteresis. The incompatibility of hysteresis with intrinsic noise in gene regulatory networks has been addressed, for example, by Lestas *et al*<sup>4</sup>. However, there are numerous works providing experimental evidence of hysteretic behaviour under significant levels of stochasticity<sup>5-8</sup>.

In the context of phenotypic switching and cell fate determination, three different scenarios have been distinguished and experimentally observed for binary decision making: deterministic *irreversible*<sup>9-11</sup>, stochastic *reversible*<sup>12</sup> and stochastic yet *irreversible* state transitioning<sup>13</sup>. Reversibility is understood here as the capacity of individual cells to switch back in absence of external signals. According to a pseudo-potential interpretation, dynamics are directed by a pseudo-

potential landscape divided by a separatrix into two basins of attraction such that each local minimum corresponds to a specific cellular state. Stochastic irreversible transitions are found to appear when cells are initialized on (or near) the separatrix<sup>13</sup>.

In this article we provide a quantitative description of hysteresis and apparent irreversibility in stochastic gene regulatory networks at the single cell level as transient effects, which disappear at the stationary state. Our analysis is based on an accurate approximation of the CME. This means that our results are valid for purely stochastic regimes far from the thermodynamic limit, and thus complementary to those based on the classical linear noise approximation which are suitable for systems near the thermodynamic limit<sup>4,14</sup>. Since the stationary solution of the CME is unique<sup>3</sup>, if the solution corresponds to a bimodal distribution, state transitions at the single cells level occur necessarily in a random and spontaneous manner, switching back and forth between regions of high probability.

Fang et al<sup>15</sup> experimentally determined an energy potential-like landscape as the negative logarithm of the probability distribution, as well as the transition rates, based on previous theoretical studies<sup>16</sup>. In this contribution, we provide a theoretical basis that explains coexistence of different expression states. In fact, under the assumption of protein bursting<sup>17</sup>, we propose an efficient form of the CME<sup>17,18</sup> that allows us to construct a meaningful probability based landscape. Furthermore, a clear link between the characteristic kinetic parameters of regulation dynamics and the resulting landscape is established.

## 2 Results

We consider the simplest gene regulatory motif exhibiting hysteresis, a single gene with positive self-regulation (see Fig. S1). In its deterministic description, the evolution of the amounts of *mRNA* and protein *X* ( $m$  and  $x$ , respectively) for the self-regulatory gene network is given by the set of ODEs:

$$\frac{dm}{dt} = k_m c(x) - \gamma_m m \quad (1)$$

$$\frac{dx}{dt} = k_x m - \gamma_x x, \quad (2)$$

where  $\gamma_m$  and  $\gamma_x$  are the *mRNA* and protein degradation rates, respectively.  $k_m c(x)$  is the transcription rate, that is essentially proportional to the input function  $c(x)$  which collects the expression from the activated and inactivated promoter states. This function incorporates the effect of protein self-regulation and takes the form<sup>19,20</sup>:

$$c(x) = (1 - \rho(x)) + \rho(x)\varepsilon, \quad (3)$$

with  $\rho(x)$  being a Hill function<sup>21</sup> that describes the ratio of promoter in the inactive form as a function of bound protein:

$$\rho(x) = \frac{x^H}{x^H + K^H}. \quad (4)$$

The above expression, can be interpreted as the probability of the promoter being in its inactive state, where  $K = k_{\text{off}}/k_{\text{on}}$  is the equilibrium binding constant and  $H \in \mathbb{Z} \setminus \{0\}$  is an integer (Hill coefficient) which indicates whether protein *X* inhibits ( $H > 0$ ) or activates ( $H < 0$ ) expression. Finally, expression (3) includes basal transcription or leakage with a constant rate  $\varepsilon = k_\varepsilon/k_m$  (see

Fig.1) typically much smaller than 1. The parameters of the Hill function employed along the paper are  $H = -7$  (the value taken from <sup>22</sup>) and  $K = 100$ , whereas  $\varepsilon = 0.05$ . Unless other value is indicated, we use  $a = 54$ . Assuming that *mRNA* degrades faster than protein *X* we have that  $m^* = k_m c(x)/\gamma_m$  and model (1) reduces to:

$$\frac{dx}{d\tau} = -x + abc(x), \quad (5)$$

where  $\tau = t\gamma_x$ ,  $a = k_m/\gamma_x$  and  $b = k_x/\gamma_m$ .

The self-regulatory network described by the deterministic equations (1-2) shows bistability and hysteresis (see Fig. 1). For a range of the control parameter,  $b$ , the system evolves towards one stable state or another depending on the initial conditions. We therefore say that the system has *memory*, since steady state values provide information about the system's past. In systems with hysteresis (dependency of the state of the system on its past), forward and reverse induction experiments follow different paths resulting in a hysteresis loop (the system switches back and forth for different values of the control parameter)<sup>23</sup>.

Gene expression is inherently stochastic. Taking into account that *mRNA* degrades faster than protein *X* in most prokaryotic and eukaryote organisms<sup>24</sup>, protein is assumed to be produced in bursts<sup>19,20,25,26</sup> at a frequency  $a = k_m/\gamma_x$ , (see equation (5)). From this assumption, it follows<sup>20,26</sup> that the temporal evolution of the associated probability density function  $p : \mathbb{R}_+ \times \mathbb{R}_+ \rightarrow \mathbb{R}_+$  can be described by a Partial Integro-Differential Equation (PIDE) of the form:

$$\frac{\partial p(\tau, x)}{\partial \tau} - \frac{\partial [xp(\tau, x)]}{\partial x} = a \int_0^x \omega(x-y)c(y)p(\tau, y) dy - ac(x)p(\tau, x), \quad (6)$$

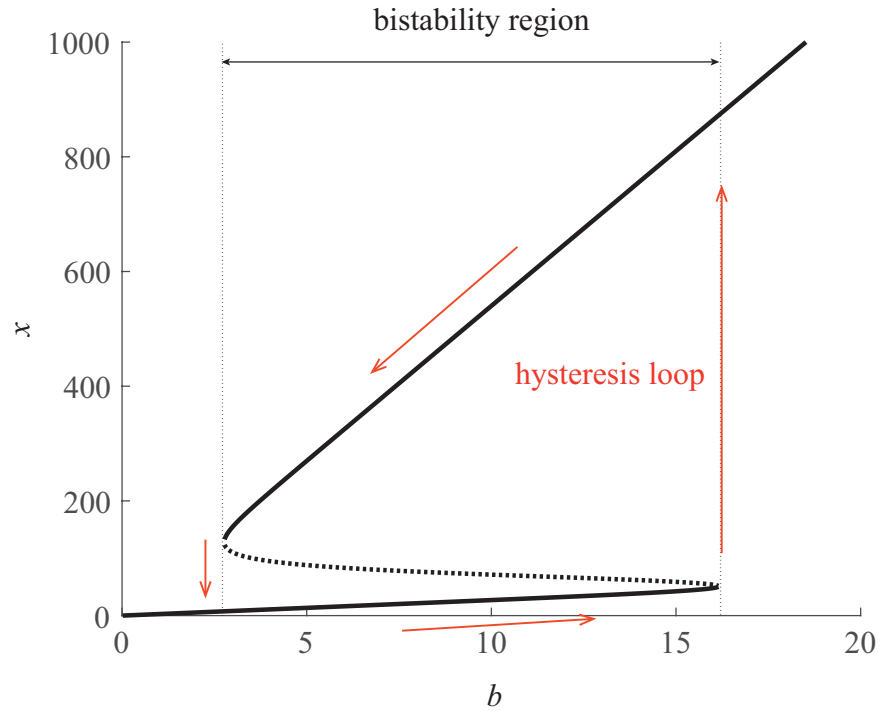


Figure 1: Hysteresis loop of the deterministic self-regulatory system. For values of the control parameter  $b$  below a given threshold, there is a unique stable steady state of low protein  $x$  towards which the system evolves independently of the initial conditions. For input signals above a second threshold, the system evolves towards a unique stable steady state of high  $x$ . For signal values within both thresholds, the system is bistable, and evolves towards one stable state or another depending on the initial conditions. In the bistability region, enclosed by two saddle-node bifurcations, three different steady states coexist (stable and unstable branches are depicted using solid and dotted lines, respectively) for a given  $b$ .

where  $x$  and  $\tau$  correspond with the amount of protein and dimensionless time, respectively. The latter variable is associated to the time scale of the protein degradation, as in the previous deterministic description. In addition,  $\omega(x - y)$  is the conditional probability for protein level to jump from a state  $y$  to a state  $x$  after a burst, which is proportional to:

$$\omega(x - y) = \frac{1}{b} \exp \left[ \frac{-(x - y)}{b} \right], \quad (7)$$

with  $b$ , as in equation (5), representing the burst size. The stationary form of the one dimensional equation (6) has analytical solution<sup>19,20</sup>  $p^*(x) = C [\rho(x)]^{\frac{a(1-\varepsilon)}{H}} x^{-(1-a\varepsilon)} e^{\frac{-x}{b}}$  where  $\rho(x)$  is defined in (4) and  $C$  is a normalizing constant such that  $\int_0^\infty p^*(x) = 1$ . It has been shown that the equilibrium solution associated to a CME is unique and stable<sup>3</sup>. This is also the case for the Friedman equation (6) whose stability has been recently proved by entropy methods<sup>27,28</sup>, which eventually makes it to qualify as a master equation itself. It is important to remark that stability properties remain valid for higher dimensions (i.e. multiple genes and proteins). While the mean  $x$ -values of the stationary solution do not depend on the initial conditions, the means obtained at the transients depend on the initial number of proteins (Fig. 2).

Note that under sufficiently slow dynamics, transient values may look stationary, thus leading to plots (red and blue lines) that resemble hysteresis, as different mean values coexist within a given interval of the  $b$  parameter. Interestingly, this interval coincides with bimodal distributions in which the two most probable states are separated by a region, in the protein space, with very low probability. This explains recent experimental observations<sup>29</sup> in which the range of apparent hysteresis was found to shrink with time. Here we denote this phenomenon as transient hysteresis and show how, in fact, the low probability region acts as a barrier that hinders transitions between

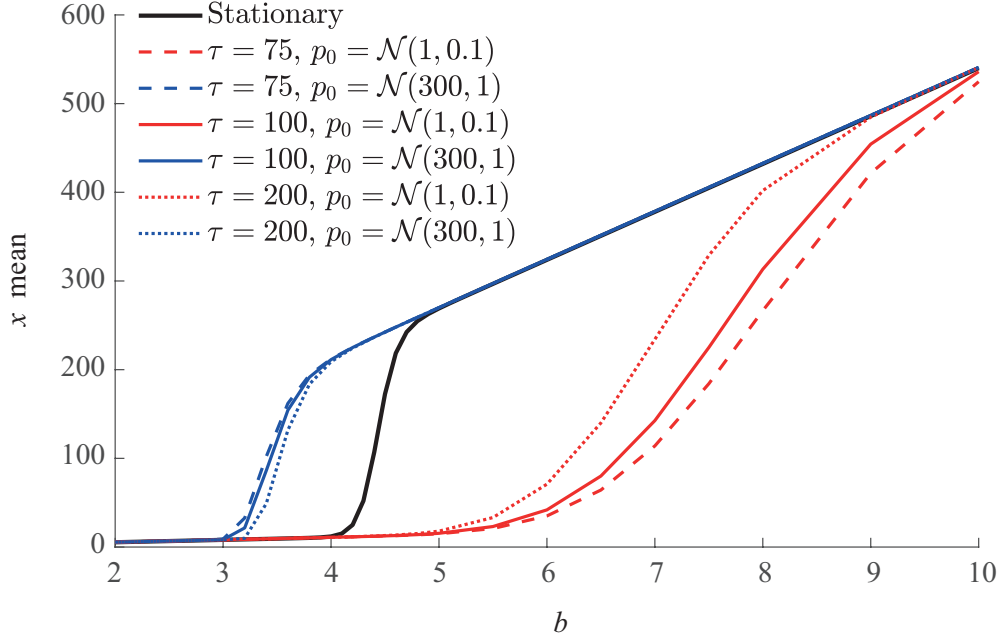


Figure 2: Slow transients lead to multiple mean states leading to a transitory hysteretic behaviour. Red and blue lines are transient solutions obtained from two different initial conditions in the form of Gaussian distributions  $\mathcal{N}(\mu, \sigma)$  with mean  $\mu$  and standard deviation  $\sigma$ . When the system achieves the stationary state (black solid line corresponds to the stationary solution of the PIDE model), there is a unique mean  $x$ -value for given  $b$  (hysteresis disappears). As time increases, the solution gets closer to the stationary distribution.



low and high protein expression, contributing in this way to slow down the dynamics towards the corresponding stationary distribution. Fig. S2 compares transient and stationary distributions for different values of the control parameter and different initial conditions. This figure provides a clear illustration of how, in presence of stochasticity, hysteresis is transitory: it shrinks with time and disappears as the system achieves the stationary state.

In order to compute an estimate of the convergence rate to equilibrium we make use of entropy methods<sup>27,28</sup> and define the entropy norm as  $G = \int_0^\infty H(u(\tau, x))p^*(x)dx$  where  $H(u(\tau, x))$  is a convex function in  $u$ , that in this study has been chosen to be  $H(u) = u^2 - 1$ , with  $u = p(\tau, x)/p^*(x)$ . According to Pájaro et al<sup>28</sup> and Cañizo et al<sup>27</sup>,  $G$  satisfies the following differential inequality:

$$\frac{dG}{dt} \leq -\eta G, \quad (8)$$

with  $\eta$  being a positive constant related to regulation (parameters  $H$  and  $K$ ), as well as the transcription-translation kinetics ( $a$ ,  $b$ ). The smaller  $\eta$ , the slower its convergence towards the corresponding equilibrium solution. Computing  $\eta$  requires a full simulation of (6) until the system reaches the equilibrium distribution for each parameter on a given range, what is computationally involved. In this work, the PIDE model (6) is solved by using the semilagrangian method implemented in the toolbox SELANSI<sup>18</sup>.

Alternatively, and in order to avoid simulation burden, we provide a truncation method to approximate the rate of convergence. The method makes use of the discrete jump process representation (see Fig. S3), which is a precursor of Friedman PIDE model, by making the protein

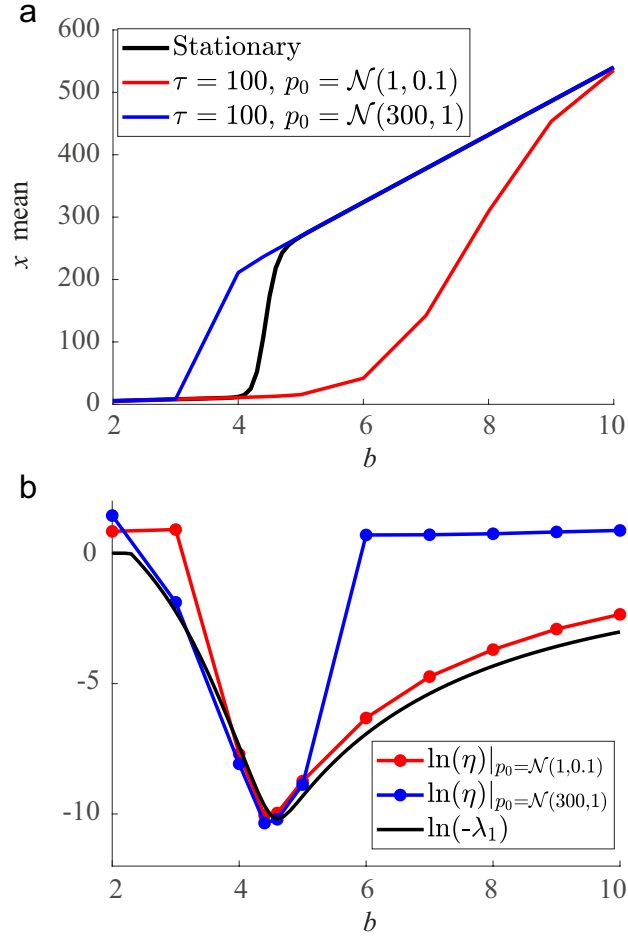


Figure 3: The parameter region leading to bimodal distributions corresponds with the slowest convergence rates a) mean  $x$ -values plotted as a function of parameter  $b$  for different initial conditions b) convergence rates of the solution towards the equilibrium distribution in logarithmic scale. Such slow dynamics is responsible for the phenomenon of transient hysteresis. If the system is allowed to achieve the equilibrium, hysteresis disappears.

amount a continuous variable<sup>17</sup>. Our method (See SI) provides a good approximation of the convergence rate  $\eta$  by the negative eigenvalue with smallest absolute value of the state change matrix  $\mathcal{M}$  associated to the discrete jump process, truncated to an  $N$  maximum number of proteins, which we refer to as  $\lambda_1$ .

Fig. 3 compares the eigenvalue  $\lambda_1$  with the convergence rate  $\eta$  obtained by simulation, for different values of the parameter  $b$ . In the parameter range where bimodal distributions occur, the negative eigenvalue  $\lambda_1$  is a good approximation of the convergence rate of the PIDE model. The figure also shows how the smaller  $\eta$  values correspond to the solution near equilibrium which lies within the hysteresis region in the  $b$  parameter space. Remarkably, low convergence rates coincide with the parameter region in which bimodal behaviour take place.

The estimation of the convergence rate (either in terms of  $\eta$  or  $\lambda_1$ ) can be obtained from kinetic coefficients  $a$  and  $b$  previously estimated from experiments. To that purpose, we can use the PIDE model to find by least squares from typically time dependent distributions obtained from a cell population by flow cytometry, the best set of parameters. Alternatively, distributions could be reconstructed from single cell time series. With the resulting model, simulations will be executed to estimate rate of convergence

This proof of concept has served to clarify how hysteresis, as it is known in deterministic nonlinear systems (i.e. as a long term stationary phenomenon) has not an equivalence in a microscopic world governed by a CME. For stochastic systems, hysteretic behaviour is a transitory phenomenon, i.e. it can be only obtained under transients that may resemble stationary solutions

due to the extremely slow dynamics at which bimodal distributions evolve.

Nonetheless, some correspondence can be drawn between the most frequently visited states on a microscopic system and the stable states on the deterministic counterpart. As it has been discussed in Pájaro et al<sup>20</sup>, the extreme states of a stationary bimodal distribution, namely those that include the highest and lowest probable states reached, satisfy:

$$-\rho(x) + \frac{-x}{ab(1-\varepsilon)} + \frac{a-1}{a(1-\varepsilon)} = 0, \quad (9)$$

where  $\rho(x)$  is defined in (4). Making zero the right hand side of equation (5) and re-ordering terms, the set of all possible equilibria satisfies:

$$-\rho(x) + \frac{-x}{ab(1-\varepsilon)} + \frac{1}{(1-\varepsilon)} = 0. \quad (10)$$

Both expressions (9) and (10) are quite similar differing only in their respective last term of the left hand side, which become closer as  $a \rightarrow \infty$ , what implies large transcription rates as compared with protein degradation. This means that the most probable states of the microscopic system are near the stable equilibrium points described by the deterministic counterpart. Moreover, they become closer as the parameter  $a$  increases.

Fig. 4 shows that the logarithm of the eigenvalue decreases as the parameters  $a$  and  $b$  become higher and smaller, respectively. Variations of the logarithm of the eigenvalue are more pronounced inside the bimodal and bistable regions. Moreover, as discussed by Pájaro et al<sup>30</sup>, as the parameter  $a$  increases the system approaches the thermodynamic limit.

These results provide us with an important insight on how to interpret experimental results

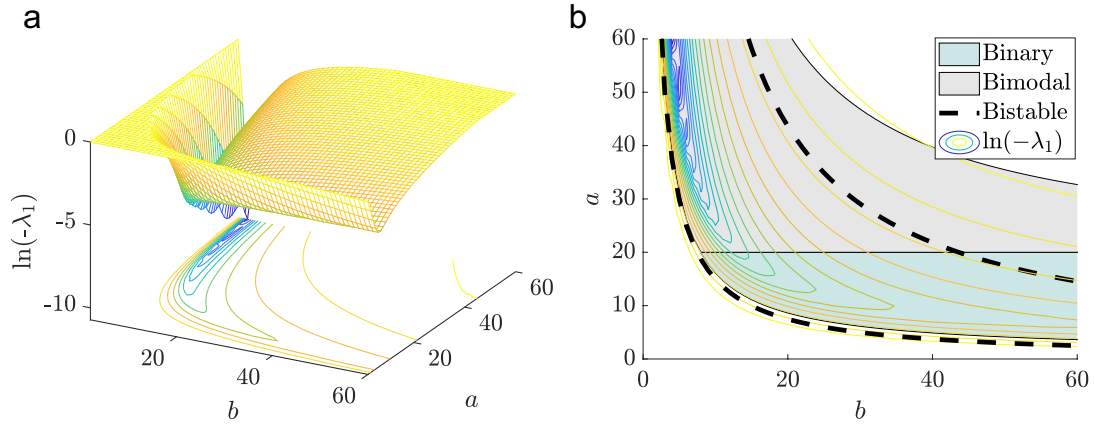


Figure 4: Evolution of the eigenvalue and bimodality (if one of the peaks lies at zero the bimodal distribution is also known as binary) and bistability regions in the parameter space (logarithmic scale) a) eigenvalue  $\lambda_1$  in the parameter space b) contour of  $\lambda_1$  in the parameter space, regions of bimodality and bistability computed by the algorithm in Pájaro et al<sup>20</sup>. The figure shows how the eigenvalue evolves with parameters  $a$ ,  $b$ .

showing hysteretic behaviour at the level of gene regulatory networks: if the system is governed by the CME, hysteresis is necessarily transient. Note that for slow dynamics (high  $a$  and low  $b$  values), the time needed to reach the stationary state might be longer than the natural timescales of relevance to the process. This is in accordance with previous studies reporting large mean passage times<sup>14</sup>, and also with Wu et al.<sup>13</sup> where they engineer a synthetic switch with stochastic yet irreversible transitions (the same mutually inhibitory gene regulatory motif is analyzed in the supplementary material using our PIDE approach).

The characterization of a cell response as hysteretic or non-hysteretic is important. For example, in a recent study concerning epithelial to mesenchymal transition (EMT), a process through which epithelial cells transdifferentiate into a mesenchymal cell fate, the authors characterize two types of responses, hysteretic and non-hysteretic EMT, and report the notable influence of hysteresis on the metastatic ability of cancer cells<sup>31</sup>.

Fig. S4 compares the set of stable and unstable equilibrium states obtained from a deterministic representation with the most and least probable microscopic states, respectively. Note that this equivalence does not support the existence of long term (stationary) hysteresis at the microscopic level. Essentially, what the picture shows is that, rather than a parameter-dependent preferential state among two stable ones, there are two highly probable states that coexist for a given parameter region on a cell population.

Invoking pseudo-potential concepts to interpret dynamics in GRN under fluctuations<sup>13</sup>, although attractive from an intuitive point of view, may be misleading since it cannot capture the

notion of coexistence. By coexistence we mean that two different protein expression levels coinciding with the peaks of the bimodal distribution coexist on a cell population (assuming no cell to cell variability on the initial conditions).

The pseudo-potential landscape is not easy to compute either, specially when increasing the number of proteins expressed. Alternatively, we can use the stationary solution of (6) to construct on the natural framework of probability distributions, a landscape informing of the possible transitions or evolution of the underlying microscopic system. As we illustrate in the example discussed in the supplementary material, its computation can be extended in a straightforward manner to larger dimensional protein spaces. This can be of used to efficiently identify most prevalent phenotypes coexisting on a given cell population.

**Data Availability:** All relevant data needed to reproduce the results are included in the text and supplementary information.

**Code availability:** The semi-lagrangian method to simulate the PIDE model is freely available and can be downloaded at: <https://github.com/selansi/Selansi>

1. Veening, J., Smits, W., & Kuipers, O. Bistability, epigenetics and bet-hedging in bacteria. *Annu. Rev. Microbiol.* **62**, 193–210 (2008).
2. Losick, R. & Desplan, C. Stochastic state transitions give rise to phenotypic equilibrium in populations of cancer cells. *Science* **320**, 65–68 (2008).

3. Van Kampen, N. G. *Stochastic Processes in Physics and Chemistry* (Elsevier, Netherlands, 2007), third edn.
4. Lestas I., R. N., Paulsson J. & G., V. Noise in gene regulatory networks. *IEEE Trans. Autom. Control* **53**, 189–200 (2008).
5. Ozbudak, E., Thattai, M., Lim, H., Shraiman, B. & van Oudenaarden, A. Multistability in the lactose utilization network of *Escherichia coli*. *Nature* **427**, 737–740 (2008).
6. Thomas, P., Popovic, N. & Grima, R. Phenotypic switching in gene regulatory networks. *Proceedings of the National Academy of Sciences USA* **111**, 6994–6999 (2014).
7. Gnügge, R., Dharmarajan, L., Lang, M. & Stelling, J. An Orthogonal Permease–Inducer–Repressor Feedback Loop Shows Bistability. *ACS Synth. Biol.* **5**, 1098–1107 (2016).
8. Hsu, C., Jaquet, V., Gencoglu, M. & Becskei, A. Protein Dimerization Generates Bistability in Positive Feedback Loops. *Cell Reports* **16**, 1204–1210 (2016).
9. Xiong, W. & Ferrell, J. A positive-feedback-based bistable memory module that governs a cell fate decision. *Nature* **426**, 460–465 (2012).
10. Wang, L. *et al.* Bistable switches control memory and plasticity in cellular differentiation. *Proc. Natl. Acad. Sci. U.S.A.* **106**, 6638–6643 (2009).
11. Ferrell, J. Bistability, bifurcations, and waddington’s epigenetic landscape. *Nature* **22(11)**, R458–R466 (2012).



12. Gupta, P. *et al.* Stochastic state transitions give rise to phenotypic equilibrium in populations of cancer cells. *Cell* **146**, 633–644 (2011).
13. Wu, M. *et al.* Engineering of regulated stochastic cell fate determination. *Proc. Natl. Acad. Sci. U.S.A.* **110**, 10610–10615 (2013).
14. Scott, M., Hwa, T. & Ingalls, B. Deterministic characterization of stochastic genetic circuits. *Proc. Natl. Acad. Sci. U.S.A.* **104**(18), 7402–7407 (2007).
15. Fang, X. *et al.* Cell fate potentials and switching kinetics uncovered in a classic bistable genetic switch. *Nature Communications* **9**, 2787 (2018).
16. Wang, J. Landscape and flux theory of non-equilibrium dynamical systems with application to biology. *Advances in Physics* **64**(1), 1–137 (2015).
17. Pájaro, M., Alonso, A. A., Otero-Muras, I. & Vázquez, C. Stochastic modeling and numerical simulation of gene regulatory networks with protein bursting. *J. Theor. Biol.* **421**, 51–70 (2017).
18. Pájaro, M., Otero-Muras, I., Vázquez, C. & Alonso, A. A. SELANSI: a toolbox for Simulation of Stochastic Gene Regulatory Networks. *Bioinformatics* **34**, 893–895 (2018).
19. Ochab-Marcinek, A. & Tabaka, M. Transcriptional leakage versus noise: A simple mechanism of conversion between binary and graded response in autoregulated genes. *Phys. Rev. E* **91**, 012704 (2015).

20. Pájaro, M., Alonso, A. A. & Vázquez, C. Shaping protein distributions in stochastic self-regulated gene expression networks. *Phys. Rev. E* **92**, 032712 (2015).
21. Alon, U. *An Introduction to Systems Biology. Design Principles of Biological Circuits* (Chapman & Hall/ CRC, London, 2007).
22. To, T. . & Maheshri, N. Noise can induce bimodality in positive transcriptional feedback loops without bistability. *Science* **327**, 1142–1145 (2010).
23. Otero-Muras, I., Yordanov, P. & Stelling, J. Chemical reaction network theory elucidates sources of multistability in interferon signaling. *PLoS Comp. Biol.* **13**, e1005454 (2017).
24. Dar, R. D. *et al.* Transcriptional burst frequency and burst size are equally modulated across the human genome. *Proc. Natl. Acad. Sci. U.S.A.* **109**, 17454–17459 (2012).
25. Ozbudak, E. M., Thattai, M., Kurtser, I., Grossman, A. D. & van Oudenaarden, A. Regulation of noise in the expression of a single gene. *Nature Genet.* **31**, 69–73 (2002).
26. Friedman, N., Cai, L. & Xie, X. S. Linking stochastic dynamics to population distribution: An analytical framework of gene expression. *Phys. Rev. Lett.* **97**, 168302 (2006).
27. Cañizo, J. A., Carrillo, J. A. & Pájaro, M. Exponential equilibration of genetic circuits using entropy methods. *J. Math. Biol.* **78**, 373–411 (2019).
28. Pájaro, M., Alonso, A. A., Carrillo, J. A. & Vázquez, C. Stability of stochastic gene regulatory networks using entropy methods. *IFAC-PapersOnLine* **49**, 1–5 (2016).

29. Hsu, C., Jaquet, V., Maleki, F. & Becskei, A. Contribution of bistability and noise to cell fate transitions determined by feedback opening. *Journal of Molecular Biology* **428**, 4115–4128 (2016).
30. Pájaro, M. & Alonso, A. A. On the applicability of deterministic approximations to model genetic circuits. *IFAC-PapersOnLine* **49**, 206–211 (2016).
31. Celi-Terrassa, T. *et al.* Hysteresis control of epithelial-mesenchymal transition dynamics conveys a distinct program with enhanced metastatic ability. *Nature Communications* **9**, 5005 (2018).

**Acknowledgements** M.P. and A.A.A. acknowledge funding from grant PIE201870E041; I.O.M. acknowledges funding from Spanish MINECO (and the European Regional Development Fund) project SYN-BIOCONTROL (grant number DPI2017-82896-C2-2-R). C.V. has been partially funded by the spanish MINECO project MTM2016-76497-R and Xunta de Galicia grant GRC2014/044.

**Author contributions** AAA, IOM conceived the research. MP, AAA performed the research. CV, MP, IOM, AAA contributed to the simulation methods. AAA, MP, IOM, CV wrote the manuscript. AAA supervised the project.

**Competing Interests** The authors declare that they have no competing financial interests.

**Correspondence** Correspondence and requests for materials should be addressed to AAA (email: antonio@iim.csic.es).

# Transient hysteresis and inherent stochasticity in gene regulatory networks

## Supplementary Information

Manuel Pájaro, Irene Otero-Muras, Carlos Vázquez and Antonio A. Alonso\*

April 3, 2019

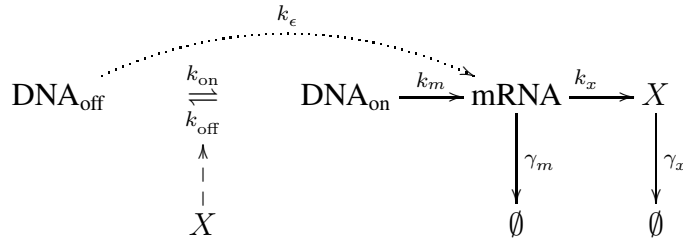


Figure S1: Self-regulatory transcription-translation mechanism. The promoter is assumed to switch between active ( $\text{DNA}_{\text{on}}$ ) and inactive ( $\text{DNA}_{\text{off}}$ ) states, with rate constants  $k_{\text{on}}$  and  $k_{\text{off}}$  per unit time, respectively. The transition is assumed to be controlled by a feedback mechanism induced by the binding/unbinding of a given number of  $X$ -protein molecules. Transcription of messenger RNA (mRNA) from the active DNA form, and translation into protein  $X$  are assumed to occur at rates (per unit time)  $k_m$  and  $k_x$ , respectively.  $k_\epsilon$  is the rate constant associated with transcriptional leakage. The mRNA and protein degradations are assumed to occur by first order processes with rate constants  $\gamma_m$  and  $\gamma_x$ , respectively.

---

\* Author to whom correspondence should be addressed. E-mail: antonio@iim.csic.es

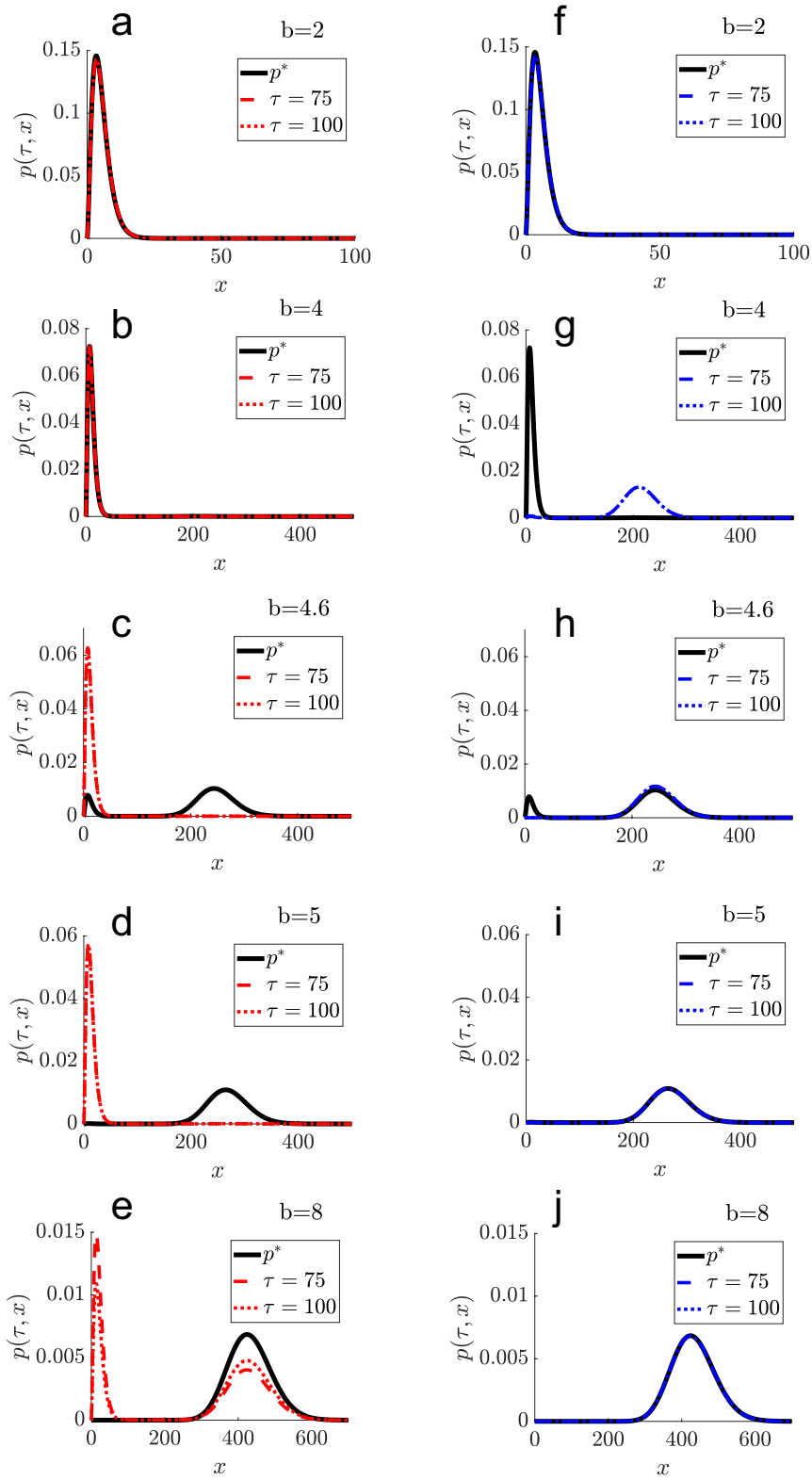


Figure S2: Stationary and transient distributions obtained for different values of the  $b$  parameter ( $a = 54$ ) for initial conditions  $p(0, x) = \mathcal{N}(1, 0.1)$  (a,b,c,d,e) and  $p(0, x) = \mathcal{N}(300, 1)$  (f,g,h,i,j). Transient distributions are represented by dashed ( $\tau = 75$ ) and dotted ( $\tau = 100$ ) lines. The black line is the stationary distribution.

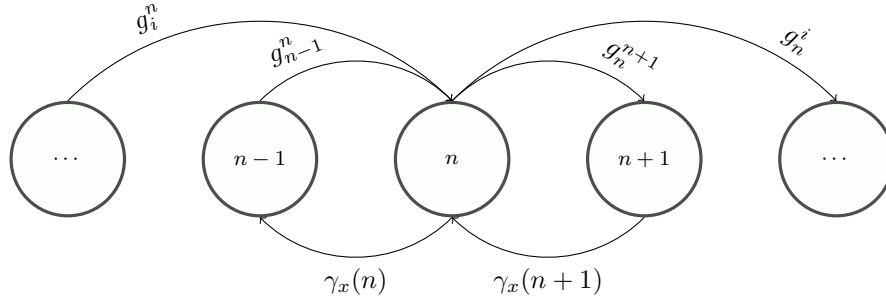


Figure S3: Jump process representation of one protein produced in bursts, where one state  $n$  can be reached from lower states  $0 \leq i < n$  with different transition probability functions  $g_i^n$ . Equivalently, from the state  $n$  the protein number can jump to higher states  $i$  with transition probability function  $g_n^i$ . The degradation follows a one step process (i. e. from state  $n$  to state  $n - 1$ ).

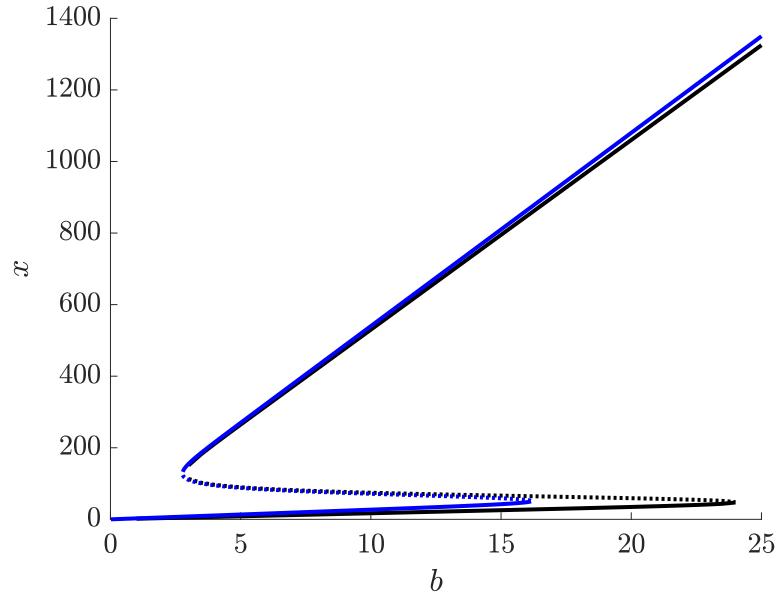


Figure S4: Equilibrium states obtained from a deterministic representation (blue lines) as compared with the extremes (maxima and minimum) of the distributions that result from a stochastic description (black lines). Blue dotted lines correspond with unstable steady states whereas black dotted lines identify the minimum of the bimodal distribution.

## A Rates of convergence (truncation method)

Here we describe a truncation method to compute the rates of convergence. Let  $\mathcal{P} : \mathbb{R}_+ \times \mathbb{N} \rightarrow [0, 1]$ , be the probability of having  $n$  proteins at time  $t$ . The time evolution of  $\mathcal{P}(t, n)$  is given by the following CME with jumps, that reads:

$$\frac{d\mathcal{P}(t, n)}{dt} = \sum_{i=0}^{n-1} g_i^n \mathcal{P}(t, i) - \sum_{i=n+1}^{\infty} g_n^i \mathcal{P}(t, n) + \gamma_x(n+1) \mathcal{P}(t, n+1) - \gamma_x(n) \mathcal{P}(t, n), \quad (\text{S1})$$

where the transition probability  $g_i^j$  is proportional to the production rate of messenger RNA, so that:

$$g_i^j := \frac{a}{b} c(i) e^{\frac{i-j}{b}}, \quad \forall j > i. \quad (\text{S2})$$

In order to obtain an approximation of the convergence rate of the PIDE model <sup>3</sup> towards the stationary state, we use the truncated form of the discrete equation (S1). Let  $N$  be the maximum possible number of proteins. Then, equation (S1) can be written in matrix form as:

$$\frac{d\mathcal{P}(t, n)}{dt} = \mathcal{M} \mathcal{P}(t, n), \quad (\text{S3})$$

where the matrix  $\mathcal{M}$  reads:

$$\mathcal{M} = \begin{pmatrix} -d_0 & \gamma_x & 0 & \cdots & 0 & 0 & 0 \\ g_0^1 & -d_1 & 2\gamma_x & \cdots & 0 & 0 & 0 \\ g_0^2 & g_1^2 & -d_2 & \ddots & 0 & 0 & 0 \\ \vdots & \vdots & & \ddots & \ddots & & \vdots \\ g_0^{N-2} & g_1^{N-2} & g_2^{N-2} & \cdots & -d_{N-2} & (N-1)\gamma_x & 0 \\ g_0^{N-1} & g_1^{N-1} & g_2^{N-1} & \cdots & g_{N-2}^{N-1} & -d_{N-1} & N\gamma_x \\ g_0^N & g_1^N & g_2^N & \cdots & g_{N-2}^N & g_{N-1}^N & -d_N \end{pmatrix}, \quad (\text{S4})$$

with the elements of the diagonal  $d_i$  being of the form:

$$d_i = \begin{cases} i\gamma_x + \sum_{n=i+1}^N g_i^n & \text{if } i = 0, \dots, N-1, \\ N\gamma_x & \text{if } i = N, \end{cases} \quad (\text{S5})$$

equivalently:

$$d_i = i\gamma_x + \frac{ac(i)}{b\left(e^{\frac{1}{b}} - 1\right)} \left(1 - e^{\frac{i-N}{b}}\right) \quad \text{for } i = 0, \dots, N. \quad (\text{S6})$$

The steady state is given by the null space of matrix  $\mathcal{M}$ , which is spanned by the normalized eigenvector associated to the unique zero eigenvalue, as the associated eigenspace has dimension one. Actually, since the graph associated to matrix  $\mathcal{M}$  (Fig. S3) has one trap, all the eigenvalues are negative except one (which is zero)<sup>2</sup>. By  $\lambda_1$ , we denote the negative eigenvalue closer to zero, i.e the one with smallest absolute value.

## B Mutual inhibitory gene regulatory motif in yeast

We consider the mutual repression gene network in<sup>1,4</sup>, where the LacI promoter is repressed by the protein expressed by the TetR promoter and vice versa, and ATc is used to inhibit the expression of TetR. Let us define  $\mathbf{x} = (x_1, x_2)$  with  $x_1$  and  $x_2$  being the amounts of LacI and TetR respectively, and  $A$  be the amount of ATc. We use the following input functions to accommodate the network to the PIDE formulation<sup>3</sup>:

$$c_1(\mathbf{x}) = C_{rl} + \frac{k_t^{n_t}}{k_t^{n_t} + \left(x_2 \left(1 + \frac{Ak_t}{k_{ATc}x_2}\right)^{-m}\right)^{n_t}}, \quad (\text{S7})$$

$$c_2(\mathbf{x}) = C_{rt} + r \frac{k_l^{n_l}}{k_l^{n_l} + x_1^{n_l}}, \quad (\text{S8})$$

where the parameters  $n_t = 1.56$ ,  $n_l = 3.35$ ,  $k_t = 11$ ,  $k_l = 264$ ,  $k_{ATc} = 0.94$ , and the degradation rate of the proteins  $\gamma_x^i = 0.002 \text{ min}^{-1}$  are taken from<sup>4</sup>. In<sup>1</sup> we find  $C_{rl} = C_{rt} = 0.005$  and



$n_t m \approx 11.5$ , so we consider that  $m \approx 7.37$ . Finally we set  $A = 4$  (because hysteresis was observed for a range of  $ATc$  between 0 and 250). We take  $\gamma_m^i$ ,  $k_m^i$  and  $k_x^i$  such that  $\frac{k_x^i k_m^i}{\gamma_m^i} = 1$  for  $i = 1, 2$ . Finally, for slow dynamics (large burst frequency, i.e. high  $a$  values) we set  $a_i = \frac{k_m^i}{\gamma_x^i} = 50$ , obtaining  $k_m^i = 0.1$ ,  $k_x^i = 0.4$  and  $\gamma_m^i = 20\gamma_x^i = 0.04$ .

We simulate the dynamics from two different initial conditions, ( $p_0 = \mathcal{N}([600, 10], 5I)$  and  $p_0 = \mathcal{N}([50, 200], 5I)$ ), and take snapshots at 50h, 100h and 150h. In Fig S5 we depict the dose-response curves at  $t=100$  for each initial condition (red and blue lines respectively) and the stationary dose response curve. It can be observed clearly how hysteresis disappears at the stationary. Note that the transient hysteresis observed at  $t = 100$  is in agreement with experimental observations by <sup>4</sup>.

The transient distributions are depicted in Fig. S6. Fig. S7 represents the corresponding marginal distribution for the same snapshots. As it is shown, the distribution at 50 h resembles an stationary distribution, since no significant differences are observed with those obtained at  $t=100$  and even at  $t=150$ . However, comparing those distributions with the stationary distribution (see also third row in Fig. S8), we clearly conclude that the system is not at the stationary state at all. Thus, the corresponding dose-response curve at  $t=50$  should present a transient hysteresis phenomenon. Note that as shown in Figures S8 and S9, even snapshots taken at much longer times (e.g. 1500 h) still differ significantly from the stationary solution.

The results for  $t = 50$  are coherent with the observation by <sup>4</sup> that if a trajectory starts clearly within one of the “basins of attraction” remains there for a long time. Note that the time needed to reach the stationary state might be longer than the natural timescales of relevance to the process. This is in accordance with <sup>4</sup> where the transitions are characterized as stochastic yet irreversible.

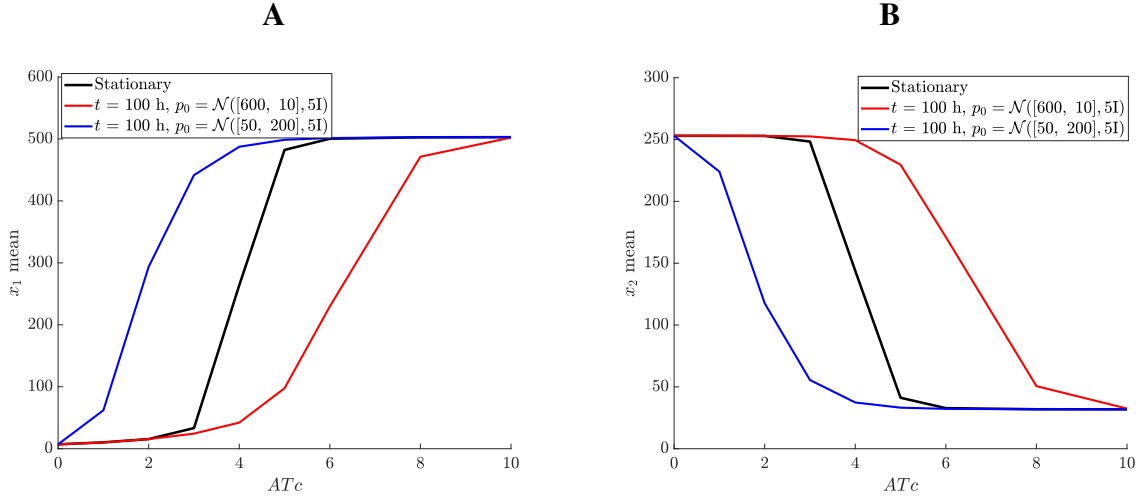


Figure S5: Slow transients lead to multiple mean states leading to a transitory hysteretic behaviour, plot A for LacI and plot B for TetR. Red and blue lines are transient solutions ( $t = 100$  h) obtained from two different initial conditions in the form of multivariate Gaussian distributions  $\mathcal{N}(\boldsymbol{\mu}, \boldsymbol{\Sigma})$  with mean vector  $\boldsymbol{\mu}$  and covariance matrix  $\boldsymbol{\Sigma}$ . When the system achieves the stationary state (black solid line corresponds to the stationary solution of the PIDE model), there is a unique mean  $x$ -value for given  $ATc$  (hysteresis disappears). Initial conditions were chosen to be near the peaks of the stationary distribution.

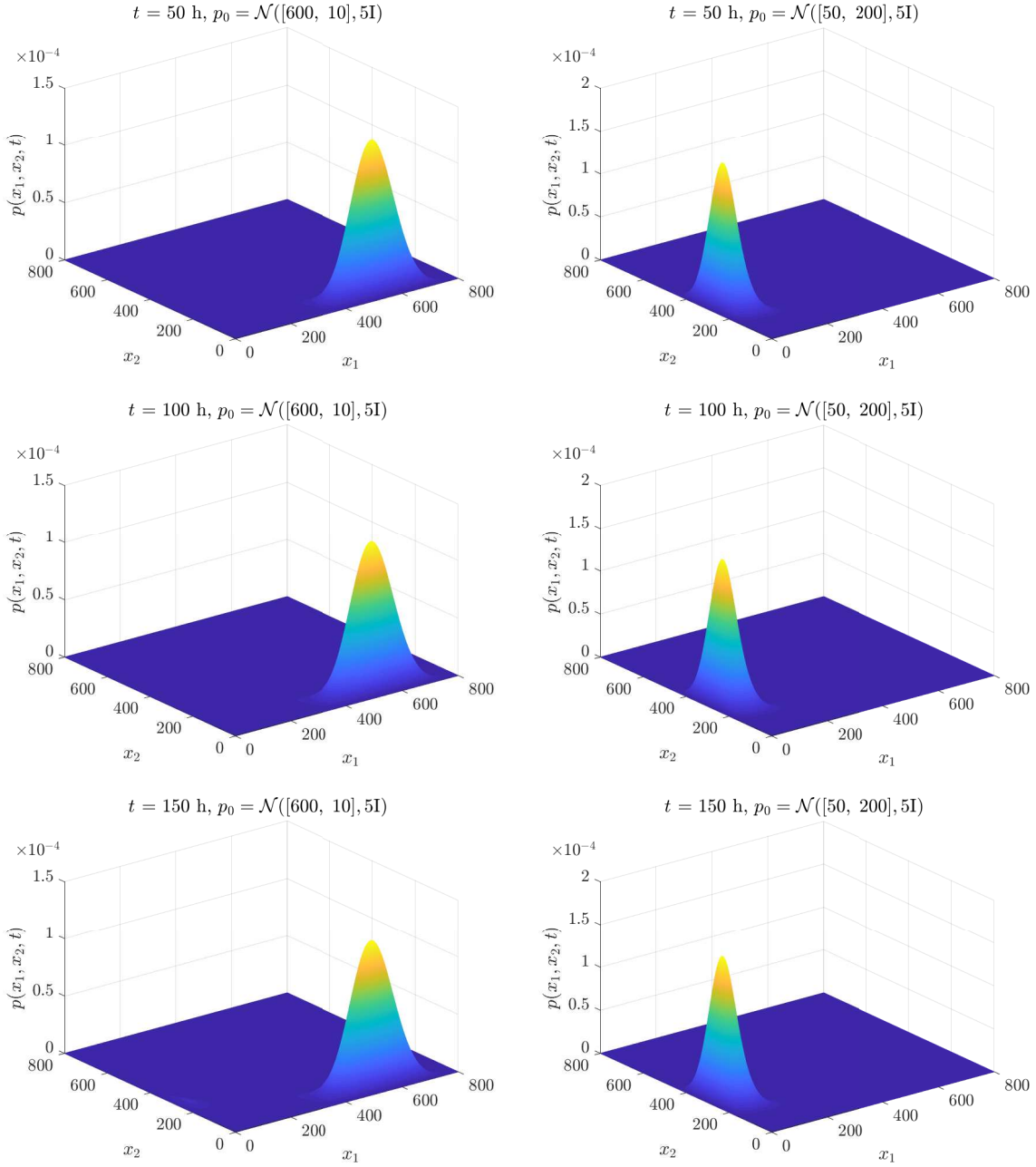


Figure S6: Transient distributions of the LacI-TetR network with initial conditions  $p_0 = \mathcal{N}([600, 10], 5I)$  (left column) and  $p_0 = \mathcal{N}([50, 200], 5I)$  (right column). Initial conditions were chosen to be near the peaks of the stationary distribution.

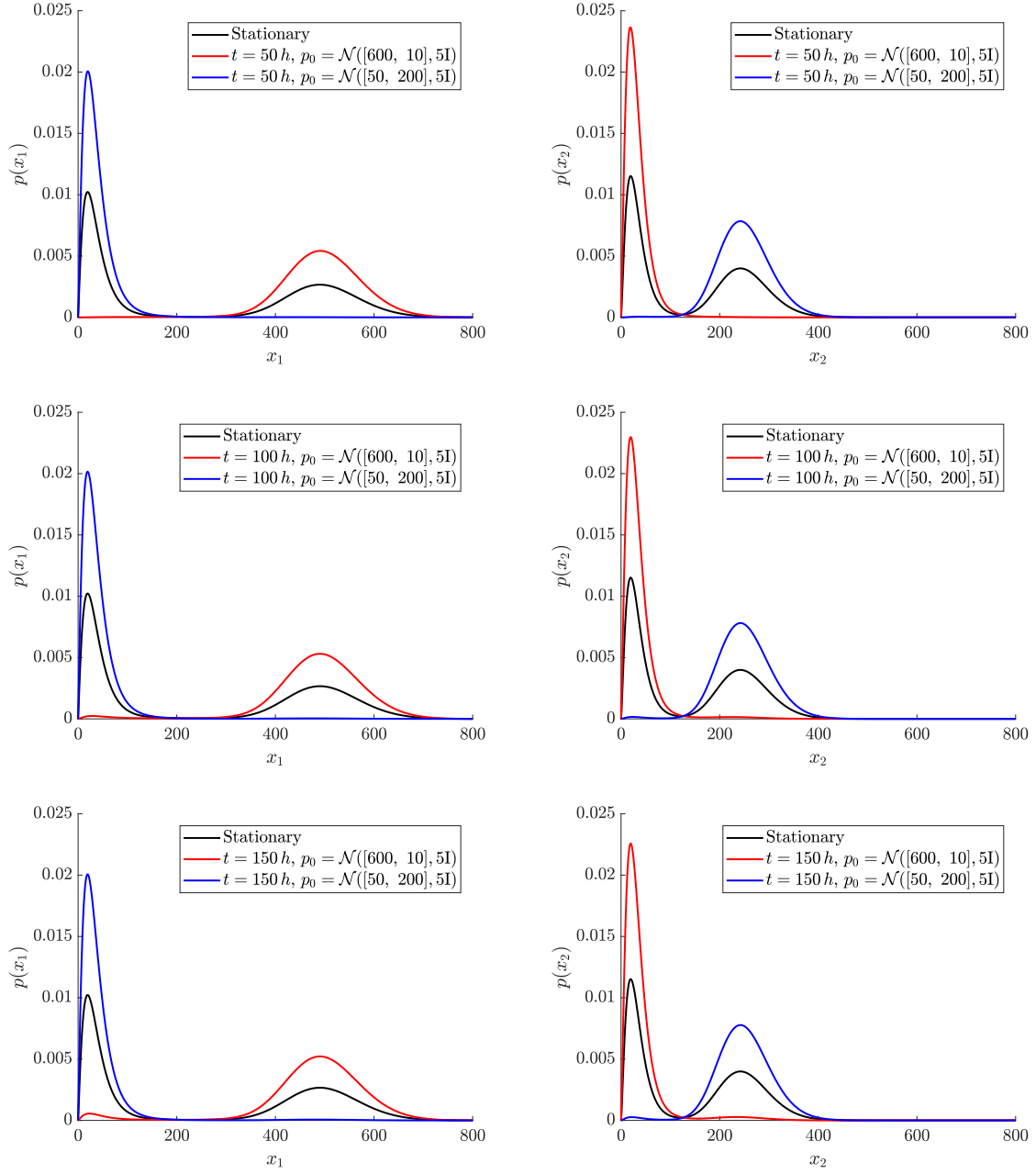


Figure S7: Stationary (black lines) and transient marginal distributions of the LacI-TetR network with initial conditions  $p_0 = \mathcal{N}([600, 10], 5I)$  (red lines) and  $p_0 = \mathcal{N}([50, 200], 5I)$  (blue lines). Marginal distributions of LacI and TetR are depicted in the first and second columns, respectively.

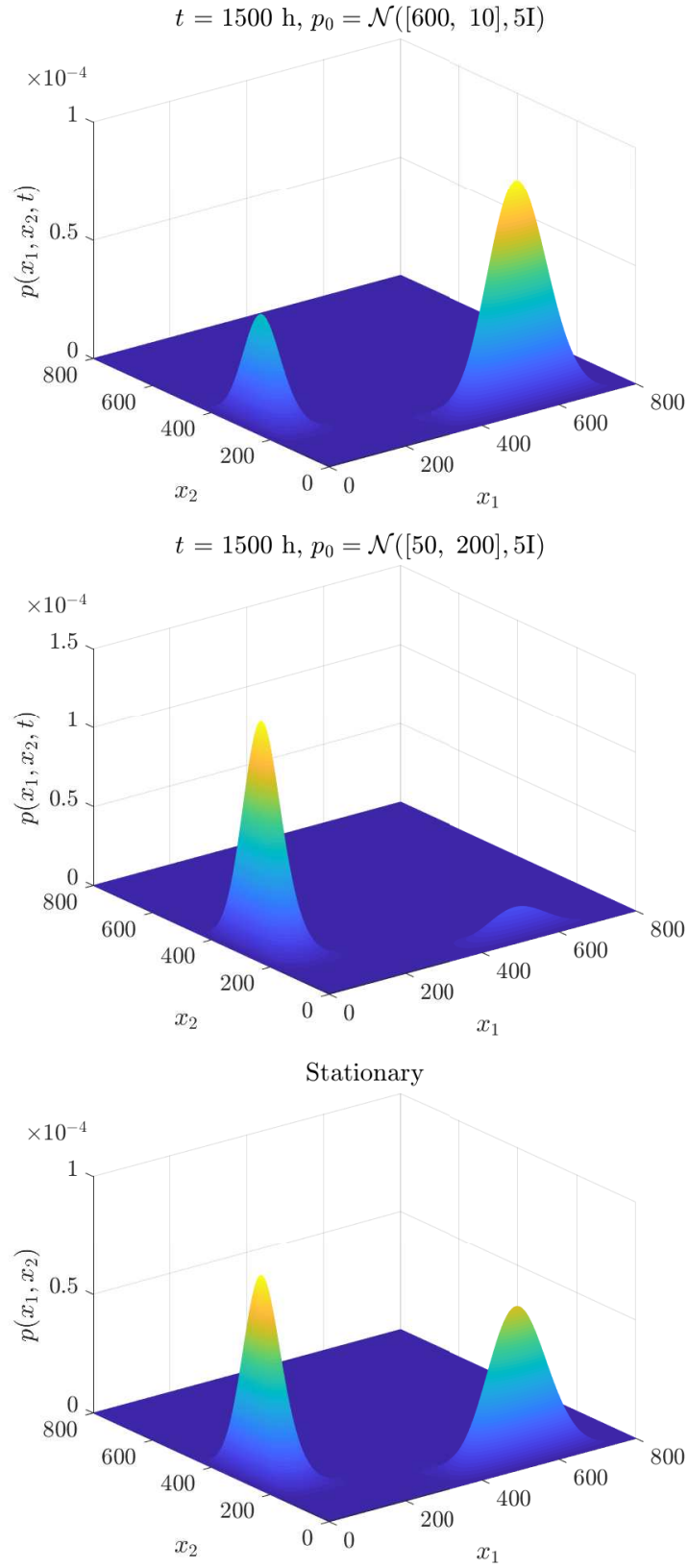


Figure S8: Stationary (third row) and transient distributions ( $t = 1500 \text{ h}$ ) of the LacI-TetR network with initial conditions  $p_0 = \mathcal{N}([600, 10], 5\text{I})$  (first row) and  $p_0 = \mathcal{N}([50, 200], 5\text{I})$  (second row). Initial conditions were chosen to be near the peaks of the stationary distribution.

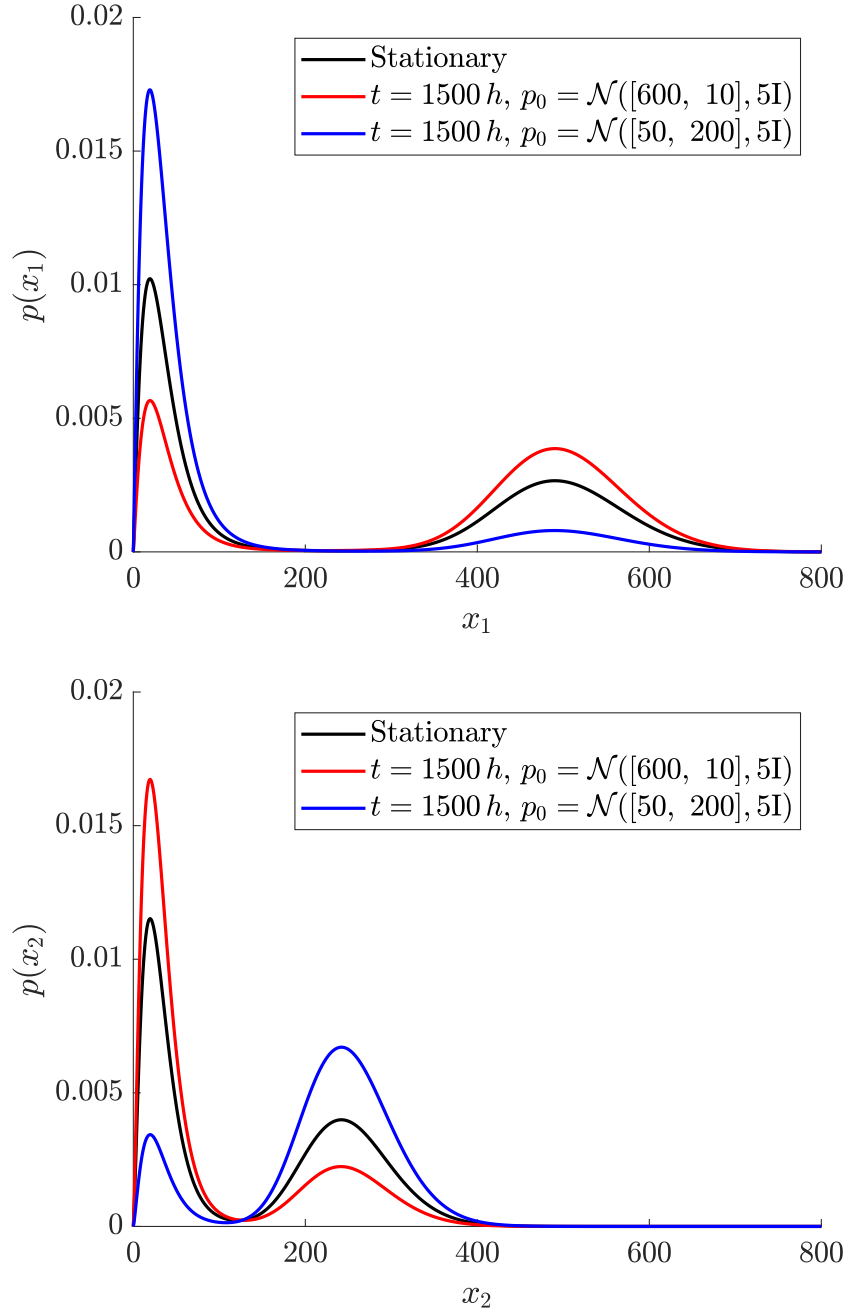


Figure S9: Stationary (black lines) and transient marginal distributions ( $t = 1500$  h) of the LacI-TetR network with initial conditions  $p_0 = \mathcal{N}([600, 10], 5I)$  (red lines) and  $p_0 = \mathcal{N}([50, 200], 5I)$  (blue lines). Marginal distributions of LacI and TetR are depicted in the first and second rows, respectively.

## References

1. T. Ellis, X. Wang, and J. J. Collins. Diversity-based, model-guided construction of synthetic gene networks with predicted functions. *Nat. Biotechnol.*, 27(5):465–471, 2009.
2. D. Fife. Which linear compartmental systems contain traps? *Math. Biosci.*, 14(3-4):311–315, 1972.
3. M. Pájaro, A. A. Alonso, I. Otero-Muras, and C. Vázquez. Stochastic modeling and numerical simulation of gene regulatory networks with protein bursting. *J. Theor. Biol.*, 421:51–70, 2017.
4. M. Wu, R. Q. Su, X. Li, T. Ellis, Y. G. Lai, and X. Wang. Engineering of regulated stochastic cell fate determination. *Proc. Natl. Acad. Sci. U.S.A.*, 110(26):10610–10615, 2013.